Iranian Journal of Astronomy and Astrophysics
Vol. 10, No. 2, Spring 2023, 201–220
©Available online at http://ijaa.du.ac.ir
DOI: 10.22128/ijaa.2023.720.1163
Online ISSN: 2383–403X

Iranian Journal of Astronomy and Astrophysics

Research Paper

Observation of Six Pre-Flare VLP Pulsations in Solar Corona

Malihe Jalalirad[1] · Narges Fathalian*[2]

[1] Department of Physics, Payame Noor University, Tehran, Iran;
email: arezoo.jalalirad@gmail.com

[2] Department of Physics, Payame Noor University, P.O.Box 19395-3697, Tehran, Iran;
*email: narges.fathalian@pnu.ac.ir

Received: 27 August 2023; **Accepted:** 28 October 2023; **Published:** 5 November 2023

Abstract. Solar flares are sudden bursts in the solar atmosphere, which emit from radio wavelengths to gamma rays, and according to their energy, are classified into different classes (A, B, C, M, and X, respectively). Predicting the time of the flare occurrence and determining its class type can help reduce its destructive effects. One of the observable structures that can be seen before a flare occurs are oscillations with very long period pulsations (VLPs) of the order of 8-30 minutes, which occur about one to two hours before the flare onset. In this paper, using GOES data, we observed typical VLPs before flare-onset for six flares in class C and M. Periodicities that we calculated for the VLPs of these flares are between 14.6 and 28.2 minutes, which is in agreement with the results of Tan et al. (2016). The number of pulses observed in each pre-flare is between 4 and 6. For the other two remaining flares of our selection, no typical pre-flare VLP was observed.

Keywords: Solar Corona, Solar Flare, Pre-flare Very Long-period (VLP) Pulsations, Flare Forecast

1 Introduction

Solar flares are sudden outbursts of emissions and radiations in the solar atmosphere, which often occur in magnetically active regions. In terms of size and energy, they range from the smallest visible phenomenon called microflares with an energy of 10^{26} erg to the largest flares with energy slightly more than 10^{26} erg [19]. The process of releasing magnetic energy in flares is done by magnetic reconnection, often created by a complex magnetic field [10]. Flares cause the acceleration of many electrons and ions and raise their energy up to relativistic energy. These accelerated particles play a significant role in releasing enormous energies from solar flares. Due to the fact that the flare is characterized by the explosion of its rays, most of them create a light spectrum and sometimes X-rays and ultraviolet rays, and they are mainly emitted by the photosphere and chromosphere in concentrated sources called Footpoints and Ribbons. These emissions and radiations are created when the lower layers of the Sun's atmosphere are heated during the flare, and this heating caused by the collision of particles probably plays an essential role in the occurrence of the flare. In addition, they also cause high-energy radiation, such as hard X-rays (HXR) from electrons and gamma

* *Corresponding author*

rays from ions. The attenuation of Alfén waves can also be substantial in heating the deep layers of the lower atmosphere where particles cannot easily penetrate. Also, the coronal radiation during the flare occurs mainly in soft X-rays and UV, but their total energy is a small fraction of the radiation energy of the radiometer. During a flare, the entanglement of a complex structure of the magnetic field with the plasma usually creates a quasi-oscillating phenomenon known as a quasi-periodic pulsation (QPP) [35]. This quasi-oscillating phenomenon can be observed in the pre-flare phase [30] or the rising and post-flare phases [21,26,29]. The reported periods in solar flares range from less than a second to several hundreds of seconds, depending on the observational instruments and wavelengths measured [23,37,38,45,59]. The general mechanism of QPP production is not yet fully known [34,51] and is attributed to magnetohydrodynamic waves [49,55] or magnetic reconnection [30,48]. According to the observations recorded so far, in the pre-flare phase, many structures, such as radio spectrum radiations, filament activity, X-ray eruptions, gamma rays, etc., have been observed and reported. By examining the observed SXR data from GOES during the pre-flare phase, it can be concluded that in some flares, one to two hours before the start of the flare, oscillations and pulses with a long period of time occur. This phenomenon, called "very long-period pulsations" (VLPs), occurs in the pre-flare phase. VLPs with similar time scales during various solar flare or even non-flare processes have been frequently reported (see for instance, [20,41,46,53,61], etc.). However, pre-flare VLPs were reported and reviewed for the first time by Tan et al. (2016) [44]. They reported four pre-flare VLPs one to two hours before the flare, for M2.9 flare on 25 October 2013, C2.4 flare on 13 July 2012, X2.0 flare on 26 October 2014, X2.7 flare on 05 May 2015 and C flares with periods ranging from 8 to 30 minutes. After that, Li et al. 2020c observed pre-flare VLPs at Hα and EUV211 wavelengths, before the occurrence of an M1.1 flare on 16 October 2015, reported to have a period of about 9.3 minutes. Jalalirad and Fathalian (2022) reported observation of Pre-flare VLP Pulsations, for 12 Solar Flares, with periods between 14 to 28.9 min [24]. In this paper, we report six flares with typical VLPs before flare-onset. First, we describe the flare classification and its phases (Section 2). Then, in Section 3, we briefly explain the methods of predicting the occurrence of solar flares. In Section 4 pre-flare VLPs and their creation mechanism is discussed in particular. Section 5 is specified in our observations and calculations. Moreover, finally, in Section 6 the conclusions are discussed.

2 Flare Classification and its Phases

Solar flares emit radiation across the electromagnetic spectrum, from radio to γ-rays, and are closely related to the acceleration of particles into interplanetary space and coronal mass ejections (CMEs). Flares occur as a result of the rapid release of energy, due to the magnetic field induced by the electric current in the corona. This energy is visible as "magnetic free energy" in the active regions, i.e., where the flare is produced. The released energy differs for different phenomena, from very small phenomena to large ones. Distribution of the number of flares, as a function of the peak energy, the total energy, or the persistence and survival of them, can be an essential factor for a better understanding of flare heating and their classification. One important classification of flares is based on their peak flux in soft X-rays (SXR) at the wavelength of 1-8 angstroms, measured by the Geostationary Orbiting Environmental Satellites (GOES). Flares are divided into categories A, B, C, M, and X. Class X flare has an energy of more than $10^{-4}Wm^{-2}$, and decreases by ten times per each class, respectively (see `https://www.nasa.gov/mission_pages/SunEarth/news/classify-flares.html`). According to this classification system, class X flares are the most powerful ones and class A flares are the weakest. Furthermore, each class of flare compared

to the flare of the next class has a 10-fold difference in released energy. Also, attributed to each type of flare, a number between 1 and 9 comes as a coefficient. For example, the X2 class flare is twice as powerful as the X1 class flare. Class C flares and smaller ones are too weak to have an impressive impact on Earth. An M-class flare can cause a short-lived radio disturbance and minor radio storms at the poles that may endanger astronauts. The largest soft X-ray flare recorded in the GOES satellite data catalog from 1975 to 2004 occurred on November 4, 2003, at 12:00 AM. This event saturated the GOES detectors, but the National Oceanic and Atmospheric Administration (NOAA) estimated that it was an X28 flare with a peak flux of $2.8\times10^{-3}Wm^{-2}$ in the 1-8 angstrom band. Of course, the powerful X-ray flux created by this flare had caused a sharp drop in the height of the ion-sphere region, which suggested that this flare was of the X45 type [43]. Previously, the classification of flares was based on the observed Hα spectra. Based on this, they used two factors of intensity and amount of radiation from the surface. Table 1 lists the classification based on X-rays and Hα (see [2,3,47]). The following phases and states usually occur in the process of the flare:

Table 1: Classification of GOES and Hα flares see [2,3,15,47]

GOES class	Peak Flux Range at 100-800 picometer (watts/square meter)	Hα class	Hα area(sq. degrees)
A	$<10^{-7}$	s	<2.0
B	10^{-7} – 10^{-6}	s	<2.0
C	10^{-6} – 10^{-5}	1	2.0
M	10^{-5} – 10^{-4}	2	5.1
X	$>10^{-4}$	3	12.4

Pre-Flare Phase- During this phase, which is about ten minutes to an hour before the flare, the intensity of soft X-rays (more than 10 KeV) increases. That is, until the time prominences in an active region become active and start to rise. In other words, minutes before the flare occurrence, the magnetic field in the active region, where the flare is occurring, begins to rearrange. Perhaps this rearrangement is due to the emergence of a new magnetic flux from the bottom of the photosphere to form new layers or the gradual relaxation of the non-potential magnetic field in the active region. This rearrangement manifests itself in three ways: 1- Preheating of gases in one or more magnetic loops, which can be observed as an increase in X-rays. 2- Increasing non-thermal movements that are observable in EUV lines 3- And the activity of the still and silent filaments and threads that are increasing along the line $H_{||} = 0$ (longitudinal magnetic field). It seems that all of these could happen without a flare, but most, if not all, flares have such effects before they occur. After rearrangement, the plasma of the active region begins to heat up so that soft X-ray and UV radiations are visible minutes before the start of the impulsive phase of the flare. During this initiation, the magnetic field in the active region destabilizes and begins to regenerate, possibly in response to the newly emerging magnetic flux. This field reconstruction leads to activating the filaments and the surrounding prominences and heating the surrounding plasma [1,36].

Impulsive Phase- The impulsive phase in a flare is characterized by rapid, intense, and variable bursts with high-energy radiations such as hard X-rays and gamma rays and at lower energies, such as EUV and optical radiations. Physically, the impulsive phase is the sudden release of stored magnetic energy in various forms such as accelerated particles, heated plasma, volume acceleration of fluid, and increased radiation. At the start of a complete flare, the impulsive phase may occur for about 100 to 1000 seconds, which includes

microwave bursts and hard X-ray bursts (over 30 KeV) caused by highly accelerated electrons. Particles that are accelerated due to heating, such as electrons, protons, and particles with heavy nuclei, enter a shock acceleration process, and a large number of particles with sub-relativistic and relativistic energies are seen during the flare. Usually, in the impulsive phase, hard X-rays are emitted from the foot points connected to the loops, and sometimes this radiation is emitted from the top of the loops, which are known as Masuda flares and have a 7 Mm long source above the hot loops [1,33].

Rise (or Flash) Phase- This phase usually lasts 5 minutes and sometimes up to 1 hour, is characterized by a sharp increase in the intensity and level of soft X-ray and Hα radiation. Acceleration of fast particles continues, and the coronal plasma reaches tens of millions of Kelvin due to heating.

Quiet Phase- In the "gradual phase" or the post-flare phase, the intensity of the flare decreases slowly (from an hour to a day). Many flares do not show a pre-flare phase, and some will have a rapid, shock explosion (for example, impulsive flares) and produce huge amounts of high-energy particles and hard X-rays. Some flares (like calm flares) have a slower process and produce less energetic radiation. Large flares start from multiple points and spread over a wide area, releasing energy from more than one region. In impulsive flares, the formation of the flare core in Hα radiation during the impulsive phase is almost simultaneous with hard X-ray bursts and microwaves. However, Hα is usually delayed by 1–2 s (and sometimes 10-20 s), which is consistent with the energy transfer by the electron beam along a loop base (in the second case, by the conducting wavefront). Sometimes, primary brightness simultaneously occurs at opposite ends of a magnetic field line. During the rise phase, knot-like bulges in the chromosphere merge to form a pair of bright Hα bands that move very fast (100 km/s) at first but soon slow down to 4 km/s, and when the flare reaches its maximum, after about 4 hours, speed reaches 1 km/s. The ribbons are associated with the rising arcs and ascending of the flare loops in the corona while they reach temperatures between 10^4K and 30 MK, and of course the cooler loops placed nested beneath the hotter loops. Since all the energy is thought to be released in the impulsive phase, these flare loops are often confused with "post-flare" loops. Nevertheless, in fact, the radiation in these loops may last up to two days in huge events, much longer than the time for the hot plasma to naturally decay by radiation or thermal conduction. Therefore, the energy release continues in the main phase. After the chromosphere reaches the corona temperature by energetic particles or wavefronts, "chromospheric evaporation" occurs, accompanied by the release of corona energy in the impulsive, rising, and quiet phases. Evaporation fills the coronal loops with hot, dense plasma. Indeed, the initial energy of the flare is transferred to the chromosphere in the form of energetic particle fall and heat transfer, causing the chromosphere plasma to heat up to the corona temperature. The slow and gradual part of the flare includes this increase in temperature, which starts with an increase in the coronal density. Then with a decrease in temperature and density, the coronal plasma is cooled and discharged downwards, towards the chromosphere [36]. The amount of energy released in flares is different. For example, for small and large flares, it is declared to be $10^{19}J(10^{26}erg)$, and $6\times10^{25}J(6\times10^{32}erg)$, respectively. This difference is related to the non-thermal nature of some flares and the accompanying coronal mass ejection in others. Hence, the radiation and energy emission in some large flares are very close to the kinetic energy of a coronal mass ejection [11,36]. Most of the total radiation appears to be during the main phase (rising phase) and a smaller fraction during the impulse phase, which are visible in the visible and UV spectrum, although they emit significantly in Hα. Part of the total energy is related to the energy of fast electrons and ions, which are converted into radiant energy in Coulomb collisions. Of course, the energy contribution of fast ions is unknown due to the unknown lower limit of ions. The energy and thermal conductivity of highly energetic

Table 2: See [36], Page 69.

Total radiant energy	2×10^{25} J (2×10^{32} erg)
Fast electrons that produce hard X-rays	2×10^{24} J (2×10^{31} erg)
Fast ions that produce γ-rays	4×10^{24} J (4×10^{31} erg)
Coronal mass ejection	2×10^{25} J (2×10^{32} erg)
Total energy output	4×10^{25} J (4×10^{32} erg)

particles contribute to optical and UV radiations.
According to the theory of Canfield et al. in 1980 [11], for a small flare, radiant energy is divided into the following parts: Later, in 2010, Kretzschmar et al. [25] measured the total

Table 3: Canfield et al. 1980 [11].

Soft X-rays (1–20 $^\circ$A)	$6 \times 10^{18} Js^{-1} (6 \times 10^{25} ergs^{-1})$
XUV lines	$2 \times 10^{18} Js^{-1} (2 \times 10^{25} ergs^{-1})$
EUV continuum	$1 \times 10^{19} Js^{-1} (1 \times 10^{26} ergs^{-1})$
Lyman α	$2 \times 10^{18} Js^{-1} (2 \times 10^{25} ergs^{-1})$
Other EUV lines	$2 \times 10^{18} Js^{-1} (2 \times 10^{25} ergs^{-1})$
Hα	$4 \times 10^{18} Js^{-1} (4 \times 10^{25} ergs^{-1})$
Other visible lines	$3 \times 10^{19} Js^{-1} (3 \times 10^{26} ergs^{-1})$
Radio continuum, cm–m wavelengths	$6 \times 10^{12} Js^{-1} (6 \times 10^{19} ergs^{-1})$

solar radiation in class M and X flares in more than one solar cycle using the SOHO/VIRGO[1] instrument. They found that irradiance is dominant in the near-UV and visible, and the total solar irradiance is typically 100 times greater than the outgoing irradiance. Of course, these sources are not enough to generate energy, and it is clear, that the main source of energy generation for flare occurrence is the magnetic field, which is stored in the nonlinear free force fields at the bottom of the corona, often around the active regions.

3 Predicting Methods for Occurrence of Solar Flares

Radiations from solar flares can often have a direct effect near the Earth, especially the Earth's ionosphere, and thus, the Earth's environment. When these flares get close to the Earth, the Earth's magnetic shield prevents them from hitting the Earth's surface, but these flares, due to their enormous energy, weaken the Earth's magnetic shield by creating magnetic storms. By weakening the Earth's magnetic shield, energetic solar particles penetrate the Earth's surface and cause climate change and sudden warming. A large solar flare can cause severe geomagnetic storms, such as powerful particle eruptions from the Sun's corona consisting of billions of tons of charged particles, which are released into interplanetary space and can reach Earth's magnetic field. Also, these magnetic changes can affect all kinds of human-made technologies. High-frequency radio waves can be attenuated and weakened:

[1]Variability of solar IR radiance and Gravity Oscillations

radios fail and GPS locators become misguided by as much as a few meters. Magnetic oscillations can also create electrical currents in the electrical grids on the ground, which can make the electrical systems expensive or overloaded during times when the power companies are not present. For these reasons, it is essential to predict the flare to reduce its harmful effects. In recent decades, the proposed methods for flare prediction have increased, and extensive evaluation is done on which one performs well. Some differences in reported achievements are due to how these achievements are measured. The differences between the presented methods in terms of performance and reaching a suitable forecast are all discussed and investigated. Thus, the prediction challenge becomes even more complicated when the flare rate is low. However, in recent years, many techniques have been presented for predicting the flare occurrence. Some methods are mentioned below briefly [8].

1- The Effective Connected Magnetic Field [18].

2- Automated Solar Activity Prediction (ASAP) [12,13].

3- Big Bear Solar Observatory/Machine Learning Techniques [60,61].

4- Total Nonpotentiality of Active Regions [14].

5- Magnetic Field Moment Analysis and Discriminant Analysis [28].

6- Magnetic Flux Close to High-Gradient Polarity Inversion Lines [42].

7- Generalized Correlation Dimension [32].

8- Magnetic Charge Topology and Discriminant Analysis [4,5,7].

9- Solar Monitor Active Region Tracker with Cascade Correlation Neural Networks [22].

10- Event Statistics [56].

11- Active Region McIntosh Class Poisson Probabilities [9,17].

In general, it is difficult to compare different studies due to the difference in data sets in the description and definition of an event since the conditions and limitations of the data required for the techniques may differ. Also, the definitions of the event in the time frame for prediction (how long a prediction can be applied), the delay time (the time between observation and prediction time), and, more fundamentally, the phenomena created in an event are different in each method. In the following, three methods have been briefly described, and the fourth method has been described in detail. These four methods are

1- Applying event statistics using the Bayesian method,

2- Automatic prediction of solar activity using hybrid software in the training machine,

3- Statistical study of the effect of magnetism on flares,

4- Observing long fluctuations before the start of a solar flare, as a sign of flare occurrence.

3.1 Applying Event Statistics Using the Bayesian Method

The best indicator for predicting upcoming flare activity is to look at past flare activity. Wheatland (2004) presents a Bayesian approach for predicting solar flares, which is based on previous observations of large and small flares and a series of specific phenomenological rules for the occurrence of flares [56]. This approach, i.e., "statistical event", has the property that it depends only on the activity of past flares and avoids the non-general choices that are implicitly used in other forecasting methods. A region that has had large flares in the past will also produce large flares in the future, called the "persistence" region, and is a reliable predictor of large flares. As an active region generates a flare, the observed flare statistics can be used to adapt the prediction for future flares based on the observational data. This method - refining guesses and probabilistic estimates based on new data - is done using Bayesian theory. The statistical study of flares has a phenomenological role in the description of the occurrence of flares, which shows that flares follow the size-power rate distribution, in which, size means some measurements of the magnitude of the flare, for example, its flux peak at the wavelength of soft X-rays. Wheatland (2004) reviewed this method for a list of soft X-ray flare data recorded in the 1-8 Å band from 1975 to 2004 [3,36].

3.2 Automatic Prediction of Solar Activity

The software Automatic Solar Activity Prediction (ASAP) provides an efficient method for predicting the physical activities of the Sun by combining machine learning and image processing methods. Computer analysis of solar images can provide automatic processing and relatively consistent performance, which uses the extensive computing capabilities of modern computing to analyze and compare data. This prediction system consists of two main modes:

a. Image processing, which processes consecutive MDI[2]/SOHO images and magnetogram to detect and classify sunspots, and extract their conditions and characteristics, which includes McIntosh classification.

b. The machine learning system continuously checks the history of sunspots and flare data.

MDI image processing and spot grouping:

A computer system that can detect sunspots and classify them based on the McIntosh classification is introduced by Colak, and Qahwaji (2008) [12]. This system provides the techniques of consecutive and continuous SOHO/MDI imaging and magnetogram images to reveal the areas containing sunspots and extract their characteristics along with the McIntosh classification for them. The extracted sunspots should be grouped, which includes the following states: (see Figure 1.)

I Sunspot detection from continuous MDI images using an intensity threshold selection.

II The detection of active region candidates from MDI magnetogram images using morphological image processing algorithms like intensity filtering, dilation, and erosion. MDI magnetic images show the intensity of the vector magnetic field flux in the line of sight in the Sun's photosphere with black and white areas representing the two opposite poles of magnetism. The dark or black areas are the negative magnetic pole (toward the Sun), and the white or light areas are the positive magnetic pole (toward the Sun).

[2]Michelson Doppler Imager

III The application of region growing to combine sunspot and active region candidates. In the region-growing technique, small areas of candidate pixels are iteratively merged according to similarity constraints. This technique is described by Colak and Qahwaji [12].

IV The use of neural networks to combine regions of opposite magnetic polarities to determine the exact boundaries of sunspot groups.

V The marking of detected sunspot groups.

3.2.1 Predicting the occurrence of a flare using a machine learning system

Research shows that solar flares are entirely dependent on sunspots and active regions. The system described is based on the history of flares and expresses it in the form of computer training rules so that it will be able to analyze recent data and provide a prediction. In this system, the neural network (NN) training algorithm is used, which has features such as McIntosh classification and the daily number of sunspots as the input of this algorithm. This algorithm has two neural networks. First, NN uses the numerical representations of the three parts of the McIntosh classification for the sunspot region under consideration together with its sunspot region as inputs (Figure 2), and it generates the probability that this sunspot region will produce a C, M, or X class solar flare in the next 24 hours. Therefore, this network has four inputs and one output, and how to use the areas of the spots and connect the flares with the spots related to them in this network has been taught.

The vector training of this neural network includes numerical values that represent the four inputs and their goals. The target represents the actual ''FLARE''/ ''NO FLARE'' cases. For example, if there is a sunspot region with a McIntosh classification of FKI and an area of 600 in millionths of the solar hemisphere that is associated with a C, M, or X class flare, then the training vector will be [0.9, 0.9, 0.5, 0.24; 0.9][8]. After the first neural network predicts the occurrence or non-occurrence of a flare, the second neural network is activated and determines the type of flare class using the new training sets of this system. For this reason, this network has four inputs and three outputs, specifically indicating the first output of the C flare, the second output of the M flare, and the third output of the X flare. These outputs have the following conditions:

- If the sunspot group is associated only with a class C flare, then the first output will be 0.9; otherwise, it will be 0.1.

- If the sunspot group is associated only with a class M flare, then the second output will be 0.9; otherwise, 0.1.

- If the sunspot group is associated only with a class X flare, then the third output will be 0.9; otherwise, 0.1.

- If the sunspot group is associated with more than one type of solar flare, all the corresponding outputs (first output for C class, second output for M class, and third output for X class) will be 0.9; otherwise, 0.1.

For example, if there is a sunspot region with a McIntosh classification of EKI and an area of 500 in millionths of the solar hemisphere that is associated only with class C and M solar flares at the same time, then the training vector will be [0.75, 0.9, 0.5, 0.20; 0.9, 0.9,0.1][8].

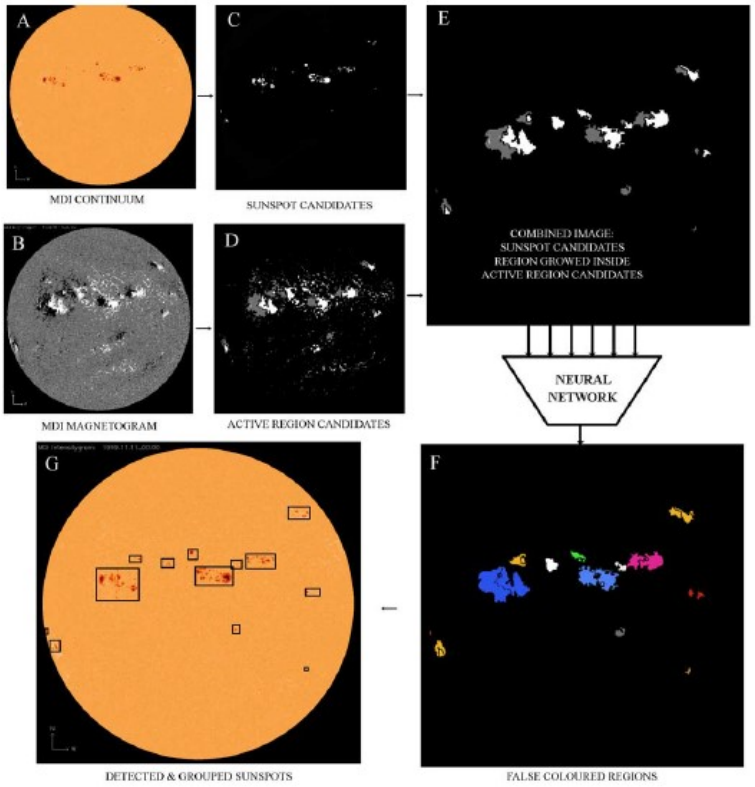

Figure 1: The stages and results of sunspot detection and the grouping process. (a and b) The continuum and magnetogram images, respectively. The (c) detected sunspots and (d) detected active regions. (e) Figures 1c and 1d are combined using region-growing to show the exact locations of the active regions. (f) Using Neural Networks, active regions are classified into groups and (g) this data is also used to detect sunspot groups [8].

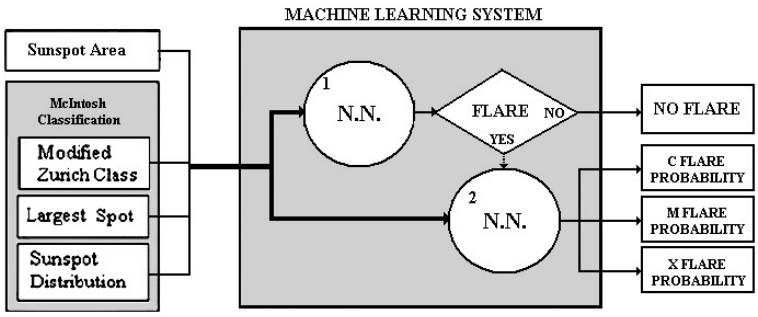

Figure 2: Machine-learning system for flare prediction [8].

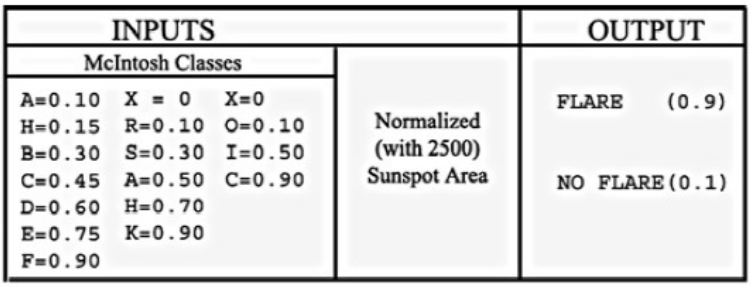

Figure 3: Input and output values for the first neural network used for determining the flaring probability [8].

3.3 Statistical Study of the Magnetic Effects on Flares, Using Vector Magnetogram of SDO/HMI

Scientists first reported a connection between the flare and changes in the photospheric magnetic field in the form of the discovery of a strong and persistent increase in the magnetic field near the Polarization inversion line (PIL) [52,54]. Also, Sudol and Harvey (2005) studied about 15 large X-class flares and concluded that the line-of-sight (LOS) magnetic field during X-class flares is constantly changing. In 2017, in the field of magnetic effects, Sun et al. conducted studies on a sample of X-class flares using the latest magnetogram vector maps with very high SDO/HMI graphics [40]. One of their most important discoveries was that the horizontal magnetic field increases near the Polarization Inversion Line (PIL), indicating that the vector magnetic field becomes more horizontal during flare eruptions [62]. The HMI and AIA of the SDO instruments provide images of vector magnetic fields and ultraviolet images, respectively, with detailed spatial and temperature information of the entire Sun. Space weather HMI Active Region Patch SHARP, where the active regions are briefly defined, implements the maps in a cylindrical coordinate system after corrections in the resolution of the images. Then, the components of the vector magnetic field, which include B_h, B_p, B_t (in the cylindrical coordinate system), are specified in the maps. The effects and signs of solar flares on the photosphere are mainly the result of an irreversible increase in the horizontal magnetic field, $B_h = \sqrt{B_p^2 + B_t^2}$. Therefore, for research in this field, it is necessary to focus only on the areas with magnetic changes, and two criteria should be observed in them:

a. Significant increase in B_h during solar flares. In order to avoid the increase caused by noises, an increased threshold of 100 G is considered.

b. A time-dependent increase in B_h associated with flares. In order to get rid of the changes unrelated to the flare, such as the emerging flux or the movement of magnetic structures, the change of B_h in the quiet photosphere is also calculated, and the areas where B_h increases both during the flare and after the flare are removed.

In 2019, Zekun Lu et al. carefully examined X-class flares with heliographic angles of less than 45 and selected 17 flares out of 13 active regions [62]. Using HMI and AIA tools on SDO, they prepared full disk images of vector magnetic fields and ultraviolet with time and space resolution and with very high quality. In the end, these results were obtained:

- 15 flares out of 17 show the effect of magnetism in the occurrence of the phenomenon.

- Among the 15 flares with magneto-influences, 13 have magneto-influences near the PIL, and 2 of the flares have magneto-influences in both the PIL and sunspot penumbras.
- According to the data obtained from AIA, the studied areas (areas with magnetic field changes greater than 100 G) can be considered as the center, the place of flare occurrence.
- The strength of the magnetic field and the inclination angle of the field line both show irreversible stepwise changes [62].

Three methods of flare occurrence prediction have been briefly stated so far. Nevertheless, in recent years, many methods and techniques have been presented to predict flares, and what distinguishes these methods is the procedure they use in predicting the time of flare occurrence. In the following, a method is described in detail which its basis for predicting the occurrence of a flare is based on examining soft X-ray electromagnetic radiation before its occurrence.

3.4 Observing Long Fluctuations Before the Start of a Solar Flare

In general, a solar flare is divided into three phases, according to the light curve of the soft X-ray flux recorded by GOES at a wavelength of 1 to 8 angstroms: pre-flare phase (before the start of the flare), the rising phase (from the beginning of the flare to the maximum point of its flux) which is also called the rising time of the flare, and the post-flare phase (the time after its maximum flux). In the pre-flare phase, which is about ten minutes to an hour before the flare, the intensity of soft X-rays ($<$ 10KeV) increases, that is, until the prominence of an active region starts to rise. In other words, minutes before the occurrence of a flare, the magnetic field in the active region where the flare is occurring begins to rearrange. The rising phase usually lasts 5 minutes (and sometimes up to 1 hour), is characterized by a sharp increase in the intensity and level of soft X-ray radiation and Hα. The acceleration of particles continues quickly, and the coronal plasma reaches tens of millions of Kelvin due to heating. In the pre-flare phase, or quiet phase, the intensity of the flare decreases slowly (from one hour to one day) [36]. During a flare, the entanglement of a complex structure of the magnetic field with the plasma usually creates a quasi-oscillating phenomenon known as a quasi-periodic pulsation (QPP) [35]. This quasi-oscillating phenomenon can be observed in the pre-flare phase [30] or the rising and post-flare phases [21,26,29]. The reported periods in solar flares range from less than a second to several hundreds of seconds, depending on the observational instruments and wavelengths measured [23,37,38,45,59]. The general mechanism of QPP production is not yet fully recognized [34,51] and is attributed to magnetohydrodynamic waves [35,49,55] or magnetic reconnection [30,48].

According to the observations recorded so far in the pre-flare phase, many structures, such as radio spectrum radiations, filament activity, X-ray eruptions, gamma rays, etc., have been observed. Analyzing these structures is a great help in studying flare prediction methods. By examining the observed SXR data from GOES during the pre-flare phase, it can be concluded that in some flares, one to two hours before the start of the flare, oscillations and pulses with a long period of time occur. This phenomenon is called "very long-period pulsations" (VLPs) in the pre-flare phase. The phenomenon of VLPs with similar time scales during various solar flare or even non-flare processes has been frequently reported (for example, look at [20,41,44,46,53,61], etc.). Tan et al. (2016) observed four pre-flare VLPs one to two hours before the flare, for M2.9 flare on 25 October 2013, C2.4 flare on 13 July 2012, X2.0 flare on 26 October 2014, X2.7 flare on 05 May 2015 and C flares with periods ranging from 8 to 30 minutes. After that, Li et al. (2020) observed pre-flare VLPs at Hα and EUV211 wavelengths, before the occurrence of an M1.1 flare on 16 October 2015,

which they reported to have a period of about 9.3 minutes [30]. In the next section, we will concentrate precisely on this topic.

4 Pre-Flare VLPs and their Creation Mechanism

What is the reason for the formation of pre-flare VLPs in the pre-flare phase? As we know, QPPs with a period of less than a second to several minutes occur at different wavelengths during the rising phase and the post-flare phase, which magnetohydrodynamic (MHD) oscillating provide explanations for the formation of QPPs. Because MHD oscillations can affect almost all aspects of the emission processes: magnetic reconnection and modulation of its rate, electron acceleration and dynamics, and plasma conditions, periods and other parameters are linked with the characteristics of the plasma and the morphology of the magnetic field. Foullon et al. (2005) reported long-period pulsations with a timescale of 8 - 12 min of X-ray radiation during solar flares [16]. They interpreted them as a periodic pumping of electrons in a compact flaring loop modulated by MHD oscillation. Some scientists suggested that such pulsations might be related to the slow-mode oscillations in large-scale coronal loops, while other research indicates that the long-period pulsations could be associated with gravity-driven solar interior modes and connected with the wave leakage of chromospheric oscillations [61]. Another possible explanation of VLPs is the thermal overstability of standing slow magnetoacoustic waves in the magnetic flux loops [27]. The MHD oscillation mode should be a suitable option to explain the formation of VLPs. However, when we use this mechanism to explain the formation of VLPs, we are faced with some serious questions: We know that flare explosions may be the cause of VLP formation during a flare, but it is not clear what in a non-explosive flare causes the oscillations before the flare onset. Also, we still do not have a clear explanation for the accumulation and storage of energy in the pre-flare phase. The solar flaring loops also have longitudinal electric currents. During the pre-flare phase, the active region of the flare source gradually stores and accumulates magnetic energy through convection in the photosphere. Convection in the photosphere can drive shearing, rotating, and twisting motions around loop footpoints and drive electric currents in the plasma loop. The electric current causes changes in the magnetic field, and these changes cause conduction in the plasma. The plasma current, which has a conductivity coefficient, causes the loop to resemble an *LRC* circuit with an electrical induction coefficient, L, an electrical resistivity, R, and an electrical capacity C. (To read more about this, see, [50]). So that

$$C = \frac{8\pi\rho s^2}{\mu_0^2 l I^2}; \qquad L = \frac{\mu_0 l}{\pi}\Big(\ln\frac{8l}{\sqrt{\mu s}} - \frac{7}{4}\Big), \tag{1}$$

Here, $\rho = n_e m_e + n_i m_i \approx n m_i$ is the plasma density in the unit of kg.m^{-3}, n is the plasma number density, S, l, and I are the cross-section (m^2), length of the plasma loop (m), and electric current (A), respectively. Such an *LRC* circuit will produce intrinsic oscillation with a period of ([44])

$$P = 2\pi\sqrt{LC} \approx 2.75 \times 10^4 \frac{s\sqrt{\rho}}{l}, \tag{2}$$

LRC-oscillation can modulate both thermal and non-thermal emission. Thermal emission effects soft X-ray emission, and non-thermal emission effects hard X-ray emission and energetic particles. As can be seen from the above relationship, the period of *LRC* oscillation is proportional to the cross-sectional area (S) and anti-proportional to the electric current (I) [44]. Assuming that in the flaring coronal loop: $n = 10^{16} m^{-3}$, $l = 5 \times 10^7 m$, and the cross-sectional radius is $r = 10^6 m$. Plus, this assumption that the periodicity of VLPs before the

flare is up to 50 minutes, the electric current will be about the order of 10^{10}. Is this estimate for electric current logical? We should keep in mind that the amount of electric current in an active region containing flare recorded by the observations of vector magnetograph has been reported up to the order of 10^{12} A [44]. Considering that an active region is always made up of tens or thousands of plasma loops, it is logical to assume that in a flare with a single plasma loop, especially in the pre-flare phase, the electric current will be in the order of 10^{10} A. Of course, during the rising phase of the flare, stronger electric currents are obtained, which can be due to the greater instability of the plasma loops of the flare in this phase. Usually, flares with a long rise time do not have pre-flare VLPs, which may be due to the relatively slow release of energy in these types of flares and the entanglement of the flare loops. Therefore, we expect to observe pre-flare VLPs with a higher probability in stronger flares with a shorter rise time.

4.1 Examining the Criteria for Determining Pre-Flare VLPs

In this section, we explain the criteria for determining and identifying pre-flare VLPs. In order to consider the observed pulses as pre-flare VLPs, they must have the following conditions: (1) occurred during 2 hours before the flare onset, (2) lasted for more than 30 minutes (duration, D > 30 min) and composed of at least 4 pulses, (3) the maximum amplitude of each pulse is higher than 2σ (σ is the standard derivation of the background temperature before the train of pulses), and (4) the time interval between adjacent pulses is called period (P), and the maximum period is shorter than two times of minimum period ($P_{max} < 2P_{min}$) and $P > 1$ min. When there is a pulsation satisfying the above criteria two hours before the flare onset, we say the flare is accompanied by pre-flare VLP, and when there is no such pulsation, we say the flare is without pre-flare VLP. When the pulses had the conditions explained above, we say that the flare is accompanied by pre-flare VLPs, and if not, we say that the flare is without pre-flare VLPs. In addition, in investigating such cases, it is better to study single flares so that the effect of other flares does not create a disturbance. A single flare, here, means that there are no flares of the same size or larger, in the 2 hours before it, or there is no wrong recorded data that affects the results [44].

5 Data and Observations

For this research, we used isolated flares in the 24-year cycle of the Sun, which were observed and recorded by soft X-rays of GOES satellite (`https://satdat.ngdc.noaa.gov/sem/goes/data/full/`) at a wavelength of 1-8 Åor 0.5-4 Åwith a cadence of 2 seconds. Each GOES satellite has two x-ray sensors that measure the Sun's x-rays in two bandwidths: 0.5-4 Å(short channel) and 1-8 Å(long channel). Measurements in these bands have been started by NOAA's Space Weather Prediction Center since 1974 and are stored in the US National Center for Environmental Information. The measuring instruments of this satellite divert the incoming electrons from the radiations so that only X-rays are measured. GOES 8-12 (GOES series I to M) and GOES 13-15 (GOS NOP series) satellites have ion cell detectors, X-ray detectors, and filters that create almost similar spectral bandwidth for both series. Although the electronics of these two series are very different, the measurements are similar in all full dynamic ranges except at deficient signal levels. For each sensor, the short wavelength is defined by the ion cell, while the long wavelength is defined by the thickness of the beryllium (Be) filter. GOES 13-15 satellite collects data with a cadence of 2.048 seconds for both channels A (short wavelength 0.5 to 4 Å) and B (long wavelength 1 to 8 Å) simultaneously. These data are stored in csv and netcdf (nc) format. Here, we extracted

six different flares from the above-mentioned data and analyzed them. We chose these flares among the flares that had a shorter rising time, because, according to the observations of Tan et al. (2016) [44], in such flares, there is a higher probability of pre-flare pulses. For this, we downloaded the data of the GOES 15 satellite in csv format. In order to prevent the repetition of primary information such as the flare class, its start and peak time, as well as the spatial position and the corresponding active region for the six flares, Table 4 shows them. The data are taken from two hours before the beginning of the flares to half an hour after they end. The individuality of flares is also taken into account. This means that until two hours before the flares, there were no flares of the same size or bigger than that. Then, using the codes we wrote with the help of MATLAB software, we drew the X-ray light curve of selected flares, shown in Figure 4. The SXR light curve is drawn at a wavelength of 1-8Åor 0.5-4Åfor flares. Figure 4 shows flares in which pre-flare pulses were observed. For each flare we obtained its periodicity with the Fast Fourier Transform (FFT) method in MATLAB). We considered the first period among the most significant ones obtained from the Fourier transform for each pre-flare. For example, in Figure 5, the curve of the periodogram (power spectrum in terms of frequency) is given for the first two flares. As can be seen in the curves in Figure 4, pulses with approximately equal time intervals occur before the beginning of the flare, which are the pre-flare VLPs. In some flares, the amplitude of the pulses increases from the beginning to the time of flare occurrence, such as the M1.2 flare on 2016/11/29, but in some of them, the pulse amplitude decreases, such as the M1.2 flare on 2017/09/04. As shown in Table 4, the periods we obtained for these VLP flares are between 14.6 and 28.2 minutes. The curves of Figure 6 are related to flares without pre-flares. In these types of flares, pre-flare pulses either are not seen or do not have the necessary conditions mentioned in the previous section. For example, flare C3.3 on 2017/04/18 has no pulse at all, and flare C4.3 on 2017/04/07 has only one pulse.

Table 4: Periods, obtained for flares with VLP (first six flares) and without VLP (the last two flares).

Row	Flares	Date of Occurrence	Start Time	Peak Time	End Time	Location	Period (min.)
1	M1.2	2016/11/29	23:29	23:38	23:40	S07E51	20.7
2	M1.0	2016/11/29	17:19	17:23	17:26	S07E55	24.9
3	M1.2	2017/09/04	05:36	05:49	06:05	S10W04	28.2
4	M1.0	2017/09/04	18:05	18:22	18:31	S07W11	14.6
5	M2.3	2017/09/05	17:37	17:43	17:51	S09W24	23.3
6	C2.7	2018-05-28	16:52	17:04	17:05	N16E24	15.8
Flares without Pre-Flare VLPs							
1	C3.3	2017-04-18	09:29	09:41	09:55	N09E84	—
2	C4.3	2017-04-07	19:42	19:49	19:52	S10W89	—

6 Discussion and Conclusion

In this paper, we randomly selected eight different flares from the M and C classes and examined them. We chose these flares from the flares that had a shorter rise time. According to the observations of Tan et al. (2016), in such flares, there is a higher probability for pre-flare pulses [44]. To do this, we downloaded GOES 15 data in csv format. Among these flares, three are in class C, and the rest are in class M. In six of them, we observed regular VLPs before the flare occurrence. Except for one, the rest were in class M. The periods

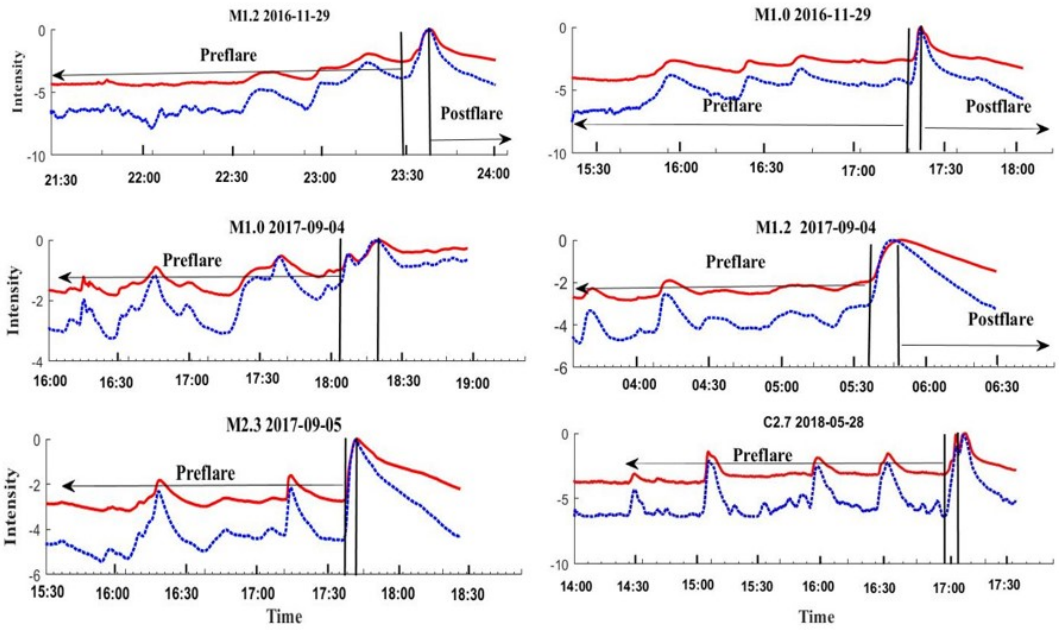

Figure 4: X-ray emission diagram of six flares in which VLP pulsations before the onset of solar flares (pre-flare VLP) have been observed. In each graph, the red curve is the light curve of the soft X-ray radiation at the wavelength of 1-8 Å, and the blue curve shows the X-ray radiation in the channel of 0.5 - 4Å. Two black vertical lines show the moment of the start and peak of the flare, and the distance between these two lines shows the rising time. These data were obtained from GOES 15 satellite. The data includes two hours before the start and half an hour after the end of the flares.

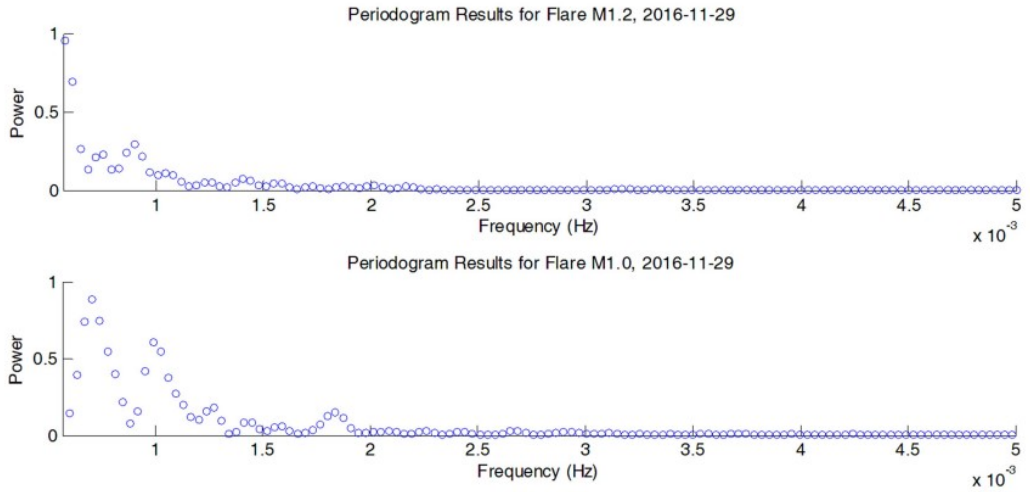

Figure 5: Periodogram curve (power spectrum in terms of frequency) for the first two flares (M1.2 and M1.0 on 2016-11-29)

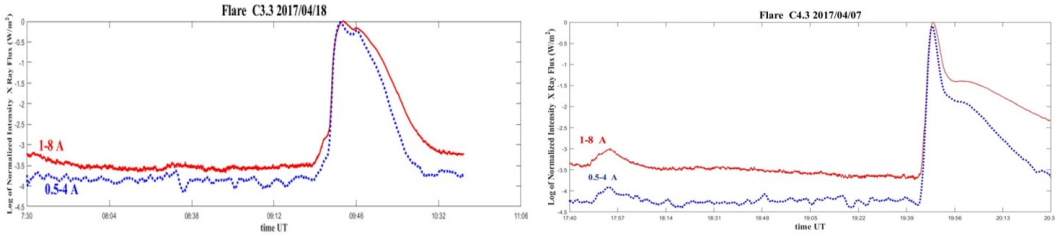

Figure 6: Flares without pre-flare VLPs.

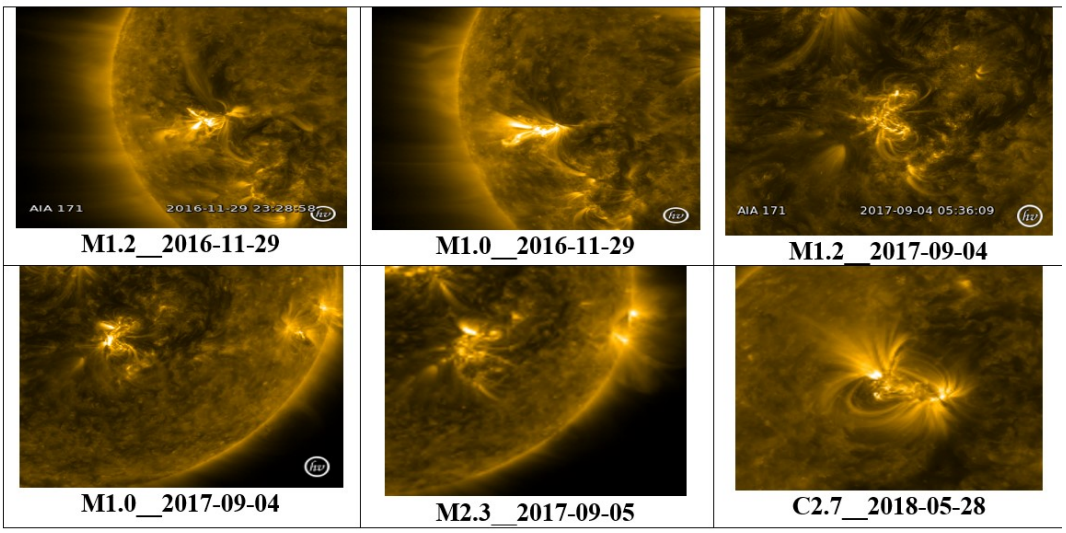

Figure 7: The active regions of the selected flares (Figure 2) taken from the AIA/SDO instrument at a wavelength of 171Å.

we observed for the VLPs of these flares are between 14.6 and 28.2 minutes, which agrees with the results of Tan et al. (2016). The number of pulses observed in each pre-flare is between 4 and 6. No regular VLP was observed for the other two of our selected flares. Pre-flare VLPs can be a precursor to the occurrence of flares. Therefore, it can be considered suitable indicator for predicting an imminent flare. Their detection and extraction are also easily possible by GOSE X-ray data, and this allows us to observe them 1-2 hours before the flare occurs. This period gives us enough time to diagnose and predict the occurrence of a flare. As mentioned before, these pulses are related to MHD oscillations. These are the quasi-periodic pulses, introduced before, with a periodicity of less than a second to several minutes that occur in different wavelengths during the rising phase and the post-flare phase. MHD oscillations provide explanations for the formation of quasi-periodic pulses. MHD oscillations can affect almost all aspects of emission and radiation processes, such as magnetic reconnection and modeling its rate of change, electron acceleration and dynamics, and plasma conditions and properties. The period and other parameters are related to the properties and characteristics of the plasma and the morphology of the magnetic field. The presence of pre-flare VLPs shows that electric currents are created in the plasma loops of the flare before the flare starts. Current-carrying loops cause plasma instabilities and X-ray radiations and ultimately produce pre-flare VLPs. Solar flare loops also have longitudinal electric currents. The electric currents located in the plasma of the loop cause changes in the magnetic field, and these changes cause conduction in the plasma. The plasma current, which has a conductivity coefficient, causes the loop to resemble an LRC circuit with an electrical inductance coefficient, L, an electrical resistivity, R, and an electrical capacity, C. As a result, the mechanism of LRC oscillations can also be a suitable explanation since the loops carrying the plasma current emit pre-flare VLPs. As mentioned, the observations show that in stronger flares with a shorter rise time, there is a greater possibility of creating pre-flare VLPs, which may be due to the relatively slow release of energy in this type of flare and the entanglement of the flare loops [44]. In all six flares in which we observed pulses or pre-flare VLPs, these VLPs report the occurrence of a flare not too long after (up to two hours later). According to our observations, the majority of flares that had VLPs were M-type flares, and the majority of C-type flares had no pre-flare; Therefore, as predicted by Tan et al. (2016), the probability of observing VLPs in larger and more energetic flares is more likely, and the occurrence of these VLPs can be considered as a mechanism for energy discharge.

Authors' Contributions

All authors have the same contribution.

Data Availability

No data available.

Conflicts of Interest

The authors declare that there is no conflict of interest.

Ethical Considerations

The authors have diligently addressed ethical concerns, such as informed consent, plagiarism, data fabrication, misconduct, falsification, double publication, redundancy, submission, and other related matters.

Funding

This research did not receive any grant from funding agencies in the public, commercial, or nonprofit sectors.

References

[1] Aschwanden, M. 2004, published in association with Prexis Publishing Chichester, UK.

[2] Bai, T., & Sturrock, P. A. 1989, ARA&A, 27, 421.

[3] Baker, D. M., 1970, 1370.

[4] Barnes, G., Longcope, D., & Leka, K. D. 2005, ApJ, 629, 561.

[5] Barnes, G., & Leka, K. D. 2006, ApJ, 646, 1303.

[6] Barnes, G., Leka, K. D., Schumer, E. A., & Della-Rose, D. J. 2007, Space Weather, 5, 9002.

[7] Barnes, G., & Leka, K. D. 2008, ApJL, 688, L107.

[8] Barnes, G., Leka, K. D., Schrijver, C. J., Colak, T., Qahwaji, R., & et al. 2016, ApJ, 829, 89B.

[9] Bloomfield, D. S., Higgins, P. A., McAteer, R. T. J., & Gallagher, P. T. 2012, ApJL, 747, L41.

[10] Benz, A. O., 2017, Flare Observations, Living Reviews in So. Ph., 14, 2.

[11] Canfield, R. C., Cheng, C. C., Dere, K. P., Dulk, G. A., McLean, D. & et al. 1980, 451.

[12] Colak, T., & Qahwaji, R. 2008, So. Ph., 248, 277.

[13] Colak, T., & Qahwaji, R. 2009, Space Weather, 7, S06001.

[14] Falconer, D. A., Moore, R. L., & Gary, G. A. 2008, ApJ, 689, 1433.

[15] Fletcher, L., Dennis, B. R., Hudson, H. S., Krucker, S., Phillips, K., & et al. 2011, SSRv, 159, 19.

[16] Foullon, C., Verwichte, E., Nakariakov, V. M., & Fletcher, L., 2005, A&A, 440, L59.

[17] Gallagher, P., Moon, Y. J., & Wang, H. 2002, So. Ph., 209, 171.

[18] Georgoulis, M. K., & Rust, D. M. 2007, ApJL, 661, L109.

[19] Hannah, G., Hudson, H. S., Battaglia, M., Christe, S., Kasparova, J., & et al. 2011, SSRv, 159, 263.

[20] Harrison, R. A., 1987, Solar soft X-ray pulsations, A&A, 182, 337.

[21] Hayes, L. A., Gallagher, P. T., Dennis, B. R., Ireland, J., Inglis, A. and Morosan, D. E., 2019, ApJ, 875, 33.

[22] Higgins, P. A., Gallagher, P. T., McAteer, R. T. J., & Bloomfield, D. S. 2011, Advances in Space Research, 47, 2105.

[23] Inglis, A. R., Ireland, J., Dennis, B. R., Hayes, L. & Gallagher, P., 2016, ApJ, 833, 284.

[24] Jalalirad, M., Fathalian, N. 2022, J. Earth and Space Physics, 48, 2, 347.

[25] Kretzschmar, M., de Wit, T. D., Schmutz, W., Mekaoui, S., Hochedez, J. F., & Dewitte, S. 2010, Nature Physics, 6, 690.

[26] Kolotkov, D. Y., Nakariakov, V. M., Kupriyanova, E. G., Ratcliffe, H. & Shibasaki, K. 2015 A&A, 574A, 53K

[27] Kumar, S., Nakariakov, V. M., & Moon, Y. J. 2016, ApJ, 824, 8.

[28] Leka, K. D., & Barnes, G. 2003, ApJ, 595, 1277.

[29] Li, D., Zhang, Q. M., Huang, Y., Ning, Z. J., & Su, Y. N., 2017, A&A, 597L4.

[30] Li, D., Li, Y., Lu, L., Zhang, Q., Ning, Z., & Anfinogentov, S. 2020, ApJ, 893, L17.

[31] Li, X., Morgan, H., Leonard, D., & Jeska, L. 2012, Astrophys. J. Letts., 752, L22.

[32] McAteer, R. T. J., Gallagher, P. T., & Conlon, P. A. 2010, Advances in Space Research, 45, 1067.

[33] Masuda, S., Kosugi, T., Hara, H., & et al. 1994, Nature, 371, 495.

[34] McLaughlin, J. A., Nakariakov, V. M., Dominique, M., Jelínek, P., & Takasao, S. 2018, Space Sci. Rev., 214, 45.

[35] Nakariakov, V. M., Kosak, M. K., Kolotkov, D. Y., Anfinogentov, S. A., Kumar, P., & Moon, Y. J. 2019, ApJ, 874, L1.

[36] Priest, E. 2014, Cambridge University Press, NewYork, NY10013-2473, USA.

[37] Pugh, C. E., Broomhall, A. M., & Nakariakov, V. M. 2019, A&A, 624, A65.

[38] Shen, Y. D., Liu, Y., Su, J. T., Li, H., Zhang, X. F., Tian, Z. J., Zhao, R. J., & Elmhamdi, A. 2013, So.Ph., 288, 585.

[39] Sudol, J. J., & Harvey, J. W. 2005, ApJ, 635, 647.

[40] Sun, X., Hoeksema, J. T., Liu, Y., Kazachenko, M., & Chen, R. 2017, ApJ, 839, 67.

[41] Svestka, Z. 1994, So.Ph., 152, 505.

[42] Schrijver, C. J. 2007, ApJL, 655, L117.

[43] Thomson, N. R., Rodger, C. J. Dowden, R. L. 2004, Geophys. Res. Lett., 31, L06803.

[44] Tan, B., Yu, Z., Huang, J., Tan, C., & Zhang Y. 2016. ApJ, 833. 206T.

[45] Tan, B., Yan, Y., Tan, C., & Liu, Y. 2007, ApJ, 671, 964.

[46] Tan, B. L., Zhang, Y., Tan, C. M., Liu, Y. Y. 2010, APJ, 723, 25.

[47] Tandberg-Hanssen, E., & Emslie, A. 1988, The Physics of Solar Flares (Chap.1), Cambridge University Press.

[48] Thurgood, J., Pontin, D., & McLaughlin, J. 2017, shin.confE. 88T.

[49] Tian, H., Young, P. R., Reeves, K. K., Wang, O., Antolin, P., Chen, B., & He, J. 2016, ApJ, 823, L16.

[50] Tobias, S. M., & Cattaneo, F. 2013, Nature, 497, 463.

[51] Van Doorsselaere, T., Kupriyanova, E. G., & Yuan, D. 2016, So. Ph., 291, 3143.

[52] Wang, H. 1992, Sol.Phys., 140, 85.

[53] Wang, H., Yuan, Y., Shih, F. Y., & Jing, J. 2011, IAU Symposium, 273, 446.

[54] Wang, H., Ewell, Jr., M. W., Zirin, H., & Ai, G. 1994, ApJ, 424, 436.

[55] Wang, T., Ofman, L., Sun, X., Provornikova, E., & Davila, J. M. 2015, ApJ, 811, L13.

[56] Wheatland, M. 2004, School of Physics, University of Sydney, NSW 2006, Australia.

[57] Wheatland, M. 2005, School of Physics, University of Sydney, NSW 2006, Australia.

[58] Yu, D., Huang, X., Wang, H., Cui, Y., Hu, Q., & Zhou, R. 2010, ApJ, 710, 869.

[59] Yu, S., & Chen, B. 2019, ApJ, 872, 71Y.

[60] Yuan, Y., Shih, F. Y., Jing, J., & Wang, H. M. 2010, RAA, 10, 785.

[61] Yuan, D., Nakariakov, V. M., Chorley, N., & Foullon, C. 2011, A&A, 533, 116.

[62] Zekun, L., Weiguang, C., Gaoxlang, J., Yining, Zh. Mingde, D., & Yang, G. 2019 arXiv:1803.08310v2 [astro-ph.SR].